Scientific Research Publishing

Open Journal of Fluid Dynamics, 2022, 12, 277-303
https://www.scirp.org/journal/ojfd
ISSN Online: 2165-3860
ISSN Print: 2165-3852

A Numerical Study of the Irradiated Ignition of Obliquely Oriented Thermally-Deformable Polymer

Shashank Singh

Independent Researcher, Chandigarh, India
Email: shashrajput@outlook.com

How to cite this paper: Singh, S. (2022) A Numerical Study of the Irradiated Ignition of Obliquely Oriented Thermally-Deformable Polymer. *Open Journal of Fluid Dynamics*, **12**, 277-303.
https://doi.org/10.4236/ojfd.2022.124014

Received: October 13, 2022
Accepted: November 27, 2022
Published: November 30, 2022

Abstract

This study numerically investigates the influence of molten matter dynamics on the gasification and subsequent ignitability of an inclined thermoplastic specimen subjected to localized irradiation heat flux normal to the surface. A thermoplastic material is modeled as a phase change material with predefined solidification and melting temperatures, respectively, and the gasification process is modeled by the Arrhenius law of molten matter. Gas phase kinetics is not considered for simplicity purposes; instead, the onset of ignition of polymer is estimated on the basis of the critical mass flux concept. According to the numerical results, as the inclination angle becomes steeper (toward the vertical angle), the estimated ignition delay becomes shorter, showing ignition is promoted, whereas it is turned to be difficult to occur when inclination angles are above the vertical angle (>90˚) having a longer delay time for the onset of gasification. With careful observation, the thermal interaction between the hot molten matter and unmelted (cold) solid is found to play an important role in gasification. The formation of a bulge due to resolidification to suppress the dripping downstream could be the source to promote ignition. By contrast, the hot molten matter is enforced to detach from the unmelted solid and "freely fall-off" to prohibit ignition for inclination angles beyond 90˚. This supports the notion that high-enthalpy caused by the external heating is simply lost because of dripping, and there is less chance of catching fire there.

Keywords

Numerical Modeling, Dripping, Resolidification, Gasification, Phase Change Material, Critical Mass Flux

1. Introduction

Polymers have been increasingly used components in residential households, industrial applications to aircraft and space engineering programs, etc. [1]. Recently, taking advantage of phase change performance at relatively low temperatures, they frequently applied as heat storage materials embedded inside a building wall [2]. Apart from such convenient and effective applications in various engineering fields, polymers are also known as one of the highly flammable (energetic) materials. Suppose that polymers are heated externally; they do melt and drip downward because of gravity drag, creating a "molten pool" beneath it. When the exposed heating is substantial, thermal decomposition would occur to evolve the volatile gas into the atmosphere. If there is a pilot source, ignition and subsequent flaming shall be experienced, which could sustain the growth of fire over the burning molten polymer by modifying its shape with time. Furthermore, dripping (hot) molten matter undergoes solidification influencing the unmelted polymers thermally throughout the entire burning process [3] [4] [5]. Zhang *et al.* (2006) found that the melting behavior of thermoplastic polymer affects the pyrolysis (gasification) process under steady-state burning. In their work, they pointed out that intensive melting would reduce the gasification rate, even though the effect of dripping was not taken into account [6]. Although no concrete reason was given, it suggests that the dynamics of molten polymers severely influence flammability properties. Unfortunately, despite recent works on this subject [7] [8] [9] [10], the effect of dynamics of molten matter during the burning event has not been elucidated; rather, it shows a random variation. This may be because the molten matter dynamics are simply difficult to reproduce the "same" process at a high repetition rate and *in-situ* measurement of thermal status is difficult. Consequently, no serious discussion could be made as to what extent the molten dynamics affects the flammability of polymers. There are limited works systematically dealing with the effect of molten dynamics on its burning character. Nakamura *et al.* studied the burning behavior of electric wire insulated with Polyethylene (PE) under normal gravity conditions and reported that molten PE significantly deformed during the burning event [11] [12]. The spread of fire damage is not limited to the region surrounding the electric wire insulation but also to the space beneath because of the dripping [13]. Furthermore, they have proposed that the size of molten matter may increase over time under microgravity, implying that the burning event shall be essentially a quasi-steady process, not a steady process [14]. For more detail, numerical approaches that include the molten matter dynamics during the burning event of the polymer are quite recommended. Such pioneering attempts have been made by Onate using the Particle Finite Element Method (PFEM) [15] [16]. Although this approach was excellent to reveal the dripping/deformation behavior of the polymers, internal heat transfer inside the molten matter cannot be handled because of the limitation of the adopted model. At nearly the same time, Kim *et al.* [17] [18] [19] [20] studied dripping dynamics by using the Enthalpy-Porosity and Volume of Fluid

method under the Finite Volume Method (FVM) to explain the complex thermal fluid process inside the molten matter. These works, have been successfully demonstrated the impact of deformation and dripping on the heat transfer rate of phase change process [17]. It is found that molten matter dynamics can accelerate dripping [18] and that the internal fluid motion by the thermocapillary effect is insignificant when the deformation is substantial [19]. By changing the orientation of the polymeric surface, the drip timing can be successfully modeled and predicted [20]. Because the primary purpose is to reveal the interaction between the dripping dynamics and melting behavior, the model did not consider gasification and the subsequent flaming process. Kandola *et al.* concluded that dripping is due to the combined effect of physical deformation, along with the pyrolysis (gasification) of polymers [21]. Other researchers revealed that under various firing configurations, molten matter dripping dramatically affects the burning behavior and vice versa [22] [23] [24] [25]. Most recently, the authors successfully integrated the gasification (pyrolysis) model into Kim's melting model, enabling them to investigate the combined effect between the gasification and molten dynamics [26]. In this work, the effect of molten viscosity has been studied over the ignitability of vertically oriented polymers through the concept of critical mass flux. It was revealed that the initiation of the gasification process in a polymeric specimen shall be strongly related to the residence time for molten matter dripping and the thermal inertia of the exposed molten matter to be ignited. Importantly, it was predicted (proposed) that bulge formation below the heating zone would be a key process for controlling ignition under locally heated conditions although this is not certain since the considered set of the parameter was insufficient to prove this prediction. This work is motivated by our previous study to prove the previously proposed methodology by controlling the inclination angle of the specimen. With variation of the inclination angle, the degree of thermal interaction between the hot molten matter and the cold (unmelted) solid is systematically altered under the condition keeping the material (thermal and dynamics) properties. Consequently, we can precisely understand the impact of thermal interaction between dripping (hot) molten matter and (cold) unmelted polymer on the material flammability, such as ignition in this study. Following the previous work, the ignitability of deforming thermoplastic material is predicted by considering the pyrolysis (gasification) process through the concept of critical mass flux.

2. Numerical Model

This work is a continuation of our previous work of authors [26], and in the work, the effect of molten dynamics over ignitability is studied by varying the inclination of polymeric surfaces only. Thus, the model descriptions, governing equations, and computational details used in this work are identical with those of the previous work [26]. Here, only a brief description of the numerical model will be made. In this study, the orientation (inclination) angle is varied as a nu-

merical parameter, and the dynamics of molten polymers and their effect on the gasification process are of the center of interest. A polymer, treated as a phase change material (PCM) in this study, is placed over an insulating material, with only one face being exposed to the atmosphere. Radiative heating is applied externally toward the exposed surface and is always placed normal to the surface, irrespective of the inclined conditions. Figure 1 shows that the inclined angle is defined as an angle between the (horizontal) baseline and the backside of the specimen. An inclination of 90˚ denotes that the heating face is vertically oriented. An inclined angle greater than 90˚ (>90˚) reveals that the heating face is located diagonally downward, whereas, an angle less than 90˚ (<90˚) shows the heating surface is placed diagonally upward.

2.1. Model Description

The computational domain is illustrated in Figure 1 and comprises a two dimensional (2D) domain that consists of a polymeric sheet (PCM) and gas. The total area of the domain is 100 mm × 44 mm, and the thickness of the PCM (d), is set to 5 mm at the right hand side of the domain over the adiabatic wall. The normal downward gravity ($\boldsymbol{g}$) with a gravitational acceleration of 9.81 m/s^2 is adopted to specify dripping upon the melting point. An irradiation source I with an intensity of 600 kW/m^2 is placed at the longways wall of D = 5 mm to initiate melting, followed by gasification. We imposed the heat flux normal to the exposed PCM surface at the heat source surface so that it was heated only at 5 mm, as described. In this work the angle of inclination for the polymer is set as α = 30˚, 75˚, 90˚, 105˚, and 120˚. Initially, all domains were maintained at a reference temperature of T_0 = 300 K. The absorption coefficient of the solid polymer

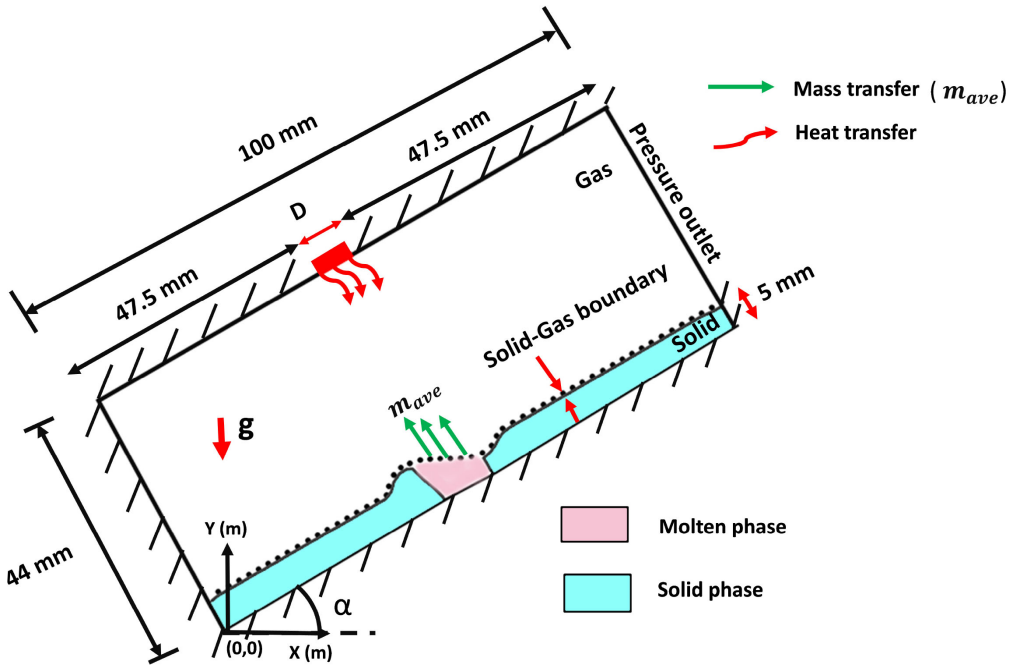

Figure 1. Numerical model considered in this study.

phase was fitted according to the Beer lambert law. Because of irradiation, the temperature inside the solid polymer increases, initiating the molten phase formation. The molten phase formation will cause a volume expansion. The molten-gas interface will deform, and the complete molten phase formation will be achieved at T_{melt} = 400 K. The solidification temperature is set at $T_{solidus}$ = 350 K. Because of deformation, the molten matter moves away from the irradiated region and re-solidifies (cools down) below its melting temperature. The portion of the polymeric material undergoing melting, resolidification, and gasification, respectively, could be identified by temperature isotherms (in the result section). With a further increase in temperature, the molten-gas interface will become a gasification surface. It is assumed that the solid is homogeneously distributed in the molten/deforming polymer, making a deformed/molten region a mushy zone. The pyrolysis/gasification is modeled as the Arrhenius type, and therefore, the rate of the gas formation increases with an increase in temperature, achieving complete gasification at 650 - 700 K [27]. Once gasification starts, the volatiles (mass flux) will transfer from the molten region toward the free surface (gas domain), please see **Figure 1**, and the mass flux is denoted by the symbol (m_{ave}).

2.2. Governing Equations

Based on the above mentioned assumptions, the set of conservation equations are described as below [26] so that we can provide the complete set of equations with brief descriptions are provided for supplemental purpose. Symbols used in this work are summarized in the nomenclature list.

2.2.1. Conservation of Volume Fraction

$$\frac{\partial \phi}{\partial t}+\nabla\cdot\left(v\phi\right)=\begin{cases}0 & \text{for non-gas}\\ M\left(-\dfrac{1}{\rho_m}\right) & \text{interface}\left(\text{gas and non-gas}\right)\text{ for } 0<\phi<1\\ 0 & \text{for gas}\end{cases} \tag{1}$$

$$M_i=\phi\times\rho_m\times A\times\exp\left(\frac{-E_a}{RT}\right) \tag{2}$$

and the total gasification rate (M) is given as:

$$M=\sum_i M_i\left(i\right) \tag{3}$$

$$\phi=\begin{cases}1=\text{molten or solid},\\ 0<\phi<1=\text{the cell contain the interface},\\ 0=\text{gas}\end{cases} \tag{4}$$

2.2.2. Conservation of Mass

$$\nabla\cdot\left(\rho v\right)=\begin{cases}\rho M\left(\dfrac{1}{\rho_g}-\dfrac{1}{\rho_m}\right) & \text{interface}\left(\text{gas and non-gas}\right)\text{ for } 0<\phi<1\\ 0 \quad \text{for gas}\end{cases} \tag{5}$$

2.2.3. Conservation of Momentum

$$\frac{\partial(\rho v)}{\partial t}+\nabla\cdot(\rho v\otimes v)=-\nabla(p)+\nabla\cdot\left[\mu\left(\nabla v+\nabla v^{\mathrm{T}}\right)\right]+\rho\boldsymbol{g}+\frac{\rho}{0.5\left(\rho_g+\rho_m\right)}\left(\sigma\kappa_c\boldsymbol{n}_s\right)\delta_s-\frac{(1-\beta)^2}{\beta^3+\varepsilon}A_{mush}v \tag{6}$$

2.2.4. Conservation of Energy

$$\frac{\partial\left(\rho\left(h+\beta L\right)\right)}{\partial t}+\nabla\cdot\left(\rho v\left(h+\beta L\right)\right)=-\nabla\cdot\left(-\lambda\nabla T+q\right)+MH_g \tag{7}$$

$$h=h_{ref}+\int_{T_0}^{T_{surf}}c_p\mathrm{d}T \tag{8}$$

ϕ is one of the phase indicators as described in Equation (4). M represents the total gasification rate defined as the sum of gasification through all gasifying polymeric cells in the unit depth direction (M_i)

In Equation (6), ρ, p and μ stand for the bulk density, pressure and the viscosity of the bulk phase, respectively. The RHS of the momentum equation consists of a series of forces subjected to the body, including the continuum surface force $\boldsymbol{F}_{ST}$ (see the fourth term of RHS), and this term is specified as a volumetric source term in the momentum equation by introducing a Dirac function. The curvature of the free surface k_c is defined through the divergence of the interfacial unit normal n_s as $\kappa_c=\nabla\cdot\boldsymbol{n}_s$. The interfacial unit normal term appears in the surface tension term, and this term determines the orientation of the curve within the cell that contains the interface $\boldsymbol{n}_s=\nabla\phi/|\nabla\phi|$ [26].

The last term on the RHS of the momentum equation is solved as a sink term and considers the mushy-region morphology by assuming that the melting front is thick and acts as a porous media [20]. In the above equation, ε is a constant with a very small value of 0.001 introduced in the equation to eliminate the numerical singularity at $\beta=0$. In this work, A_{mush} is considered a constant of the value 10^6 kg/m^3. β in the above equation is the temperature-dependent phase indicator for determining either the solid or molten phases.

$$\beta=\begin{cases}0 & \text{if } T<T_{solidus}\\ 1 & \text{if } T>T_{melt}\\ \dfrac{T-T_{solidus}}{T_{melt}-T_{solidus}} & \text{if } T_{solidus}<T<T_{melt}\end{cases} \tag{9}$$

In the case of $\beta=1$, the sink term becomes zero, and the momentum equation is solved for the molten phase. In case of $\beta\neq1$, the permeability tensor dominates, and the transient, convective and diffusive term and the momentum equation become identical with the Carman-Kozeny equation [26].

In the energy equation, h represents enthalpy of the bulk phase. In the above equation *i.e.* Equation (7), λ represents the thermal conductivity of the bulk phase. Furthermore, in the energy equation, the term $\nabla\cdot q$ represents the divergence of the radiative heat flux. This source term accounts for heat sources (or sinks) because of radiation, and the radiative heat transfer equation is solved

through the discrete ordinate (DO) radiation model.

The bulk properties of the polymeric material found in the mass, momentum, and energy conservation equation could be expressed using phase indicators, such as ϕ and β [26].

$$\begin{aligned}
\rho &= \phi\left(\rho_s + \beta\left(\rho_s - \rho_m\right)\right) + \left(1-\phi\right)\rho_g \\
\mu &= \phi\mu_m + \left(1-\phi\right)\mu_g \\
\lambda &= \phi\left(\lambda_s + \beta\left(\lambda_s - \lambda_m\right)\right) + \left(1-\phi\right)\lambda_g \\
c_p &= \phi\left(c_{p,s} + \beta\left(c_{p,s} - c_{p,m}\right)\right) + \left(1-\phi\right)c_{p,g}
\end{aligned} \tag{10}$$

Here, subscript such as s, m, and g stands for solid, molten, and gas phases, respectively. All the properties used in Equation (10) are summarized in Table 1.

Table 1. Material properties of the computational domain [26].

Parameter	Symbol	Value	Units
Air (gas phase)			
Density	ρ_g	1.225	kg/m^3
Thermal conductivity	λ_g	0.0242	W/mK
Specific heat	$c_{p,g}$	946 + 0.19 × T	J/kgK
Viscosity	μ_g	1.789 × 10^{-5}	Pa.s
PCM (solid phase)			
Density	ρ_s	980	kg/m^3
Thermal conductivity	λ_s	24	W/mK
Specific heat	$c_{p,s}$	1360	J/kgK
Latent heat of melting	L	1.8 ×10^5	J/kg
PCM (molten phase)			
Density	ρ_m	882	kg/m^3
Thermal conductivity	λ_m	15	W/mK
Specific heat	$c_{p,m}$	680	J/kgK
Viscosity	μ_m	0.1	Pa.s
Solidification temperature	$T_{solidus}$	350	K
Melting temperature	T_{melt}	400	K
Devolatilization Kinetic reaction			
Activation energy	E_a	188	kJ/kgmol
Pre-exponential factor	A	8.5 × 10^{11}	s^{-1}
Latent heat of vaporization	H_g	1.35 × 10^6	J/kg
Irradiation intensity	I	6 × 10^5	W/m^2

The gasification process is confirmed by a one-step pyrogasification reaction mechanism. Here, it is assumed that the molten polymer undergoes thermal scission, followed by gasification to produce combustible and noncombustible products. The reaction is modeled using the species transport approach [26]. The one-step gasification reaction is given by the expression.

$C_1H_{1.428}O_{0.285} \rightarrow 0.946$ [Combustible gases] + 0.054 [Non-Combustible gases]

2.3. Computational Details

To ensure the stability of the numerical simulation, the time step (Δt) [s] for the simulations is calculated through the CFL condition. The problem is modeled as transient, and the time step (Δt) is varied from 0.07 ms to 0.5 ms in order to ensure thermal stability. The convective terms in the governing equation are discretized using second-order discretization schemes, whereas the diffusive term is evaluated using the central differencing scheme. The species formation during gasification is discretized using the second-order upwind scheme. The radiation term (DO intensity) is discretized through the first-order upwind scheme. Pressure velocity coupling is modeled via the SIMPLE scheme. Interpolation of pressure at the face from the cell center values is modeled through the Pressure Staggering Option (PRESTO). The Piecewise Linear Interpolation Calculation (PLIC) method is used to calculate the transport (ϕ), and the method is used to prevent the numerical diffusion [26].

3. Numerical Results

First, let us look into the dripping dynamics at various inclination angles. **Figures 2-6** show the time-sequence of the 2D domain of temperature isotherms and melt fraction at various orientations of the polymer specimen (**Figure 2**: 30˚, **Figure 3**: 75˚, **Figure 4**: 90˚, **Figure 5**: 105˚ and **Figure 6**: 120˚). In each figure, the interface is added as a thick black continuous line and dotted lines to represent the molten matter for better readability. Note that the polymer melts at 400 K, and the gasification temperature is set as 500 K, whereas the molten polymer solidifies at 350 K.

3.1. Dripping Dynamics (Cases for 30˚)

In the case of inclination at 30˚ (see **Figure 2**), dripping gradually occurs, and since there is a relatively large amount of the molten matter to be heated, slow dripping eventually appears. The slight deformation of the molten matter starts at $t = 3$ s at which even local heating occurs at the spot. Because the density of the molten matter is lower than the virgin solid (see **Table 1**), volume expansion occurs as the molten layer spreads. As the polymer is further heated, a clear "bulge" is formed around the downward edge of the heated zone. This is because the expanded (hot) molten matter (which is above the melting temperature) cools down due to the heat dissipation into the unmelted solid. Simultaneously, conduction from the heated molten matter through the specimen to heat up in

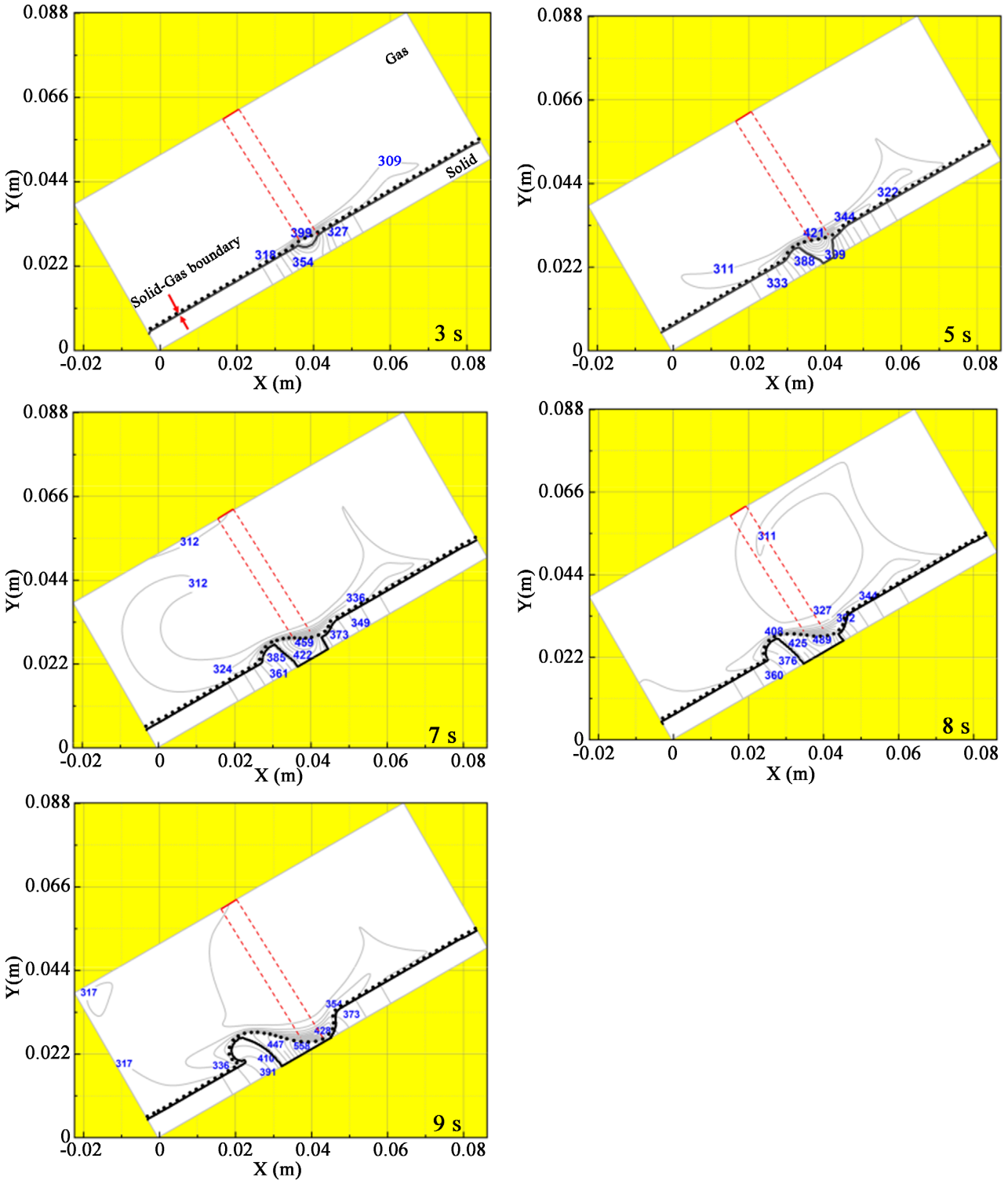

Figure 2. Temperature isotherms and melt contour for inclination of $\alpha = 30^{\circ}$.

the relatively wider zone of the solid polymer, which may expect to prohibit the further formation of the bulge. Continuous exposure further expanded the molten matter and the bulge, as shown in the figure ($t > 7$ s). Interestingly, the localized heated part remains below 500 K till $t = 7$ s, with no apparent gasification

expected (note that the intense gasification starts above 650 K based on the current pyrolysis model). Because the dynamics of the molten is less pronounced due to the presence of the bulge, the substantial molten matter stays at the heated zone, which contributes to maintaining the high thermal inertia to achieve a gentle increase in temperature. However, because the molten matter is hotter than the unmelted solid, the downstream edge of the molten-solid interface progresses slowly. As time passes, the volume (mass) of the molten matter further increases and a small amount of the molten matter floods over the bulge (like film liquid), where it is immediately cooled down by the cold solid beneath it, causing a bulge to form downstream. In this way, a slow movement of the molten matter with a downward bulge is observed. Eventually, at $t = 8.95$ s, the temperature of the molten matter at the irradiated zone reaches above 500 K, the pyrolysis reaction is gradually promoted according to the Arrhenius law (Equation (2)), and gasification is started. As shown in the figure, at $t = 9$ s, because of the progress of the downstream edge of the molten-solid interface, as described, the thickness of the molten matter at the irradiated zone reduces, the corresponding thermal inertia decreases, and the temperature of the molten matter increases further. Alternatively, gasification is promoted and reaches above the critical mass flux to initiate ignition.

3.2. Dripping Dynamics (Cases for 75˚ and 90˚)

For the case of 75˚ and 90˚ inclinations (**Figure 3** and **Figure 4**, respectively) the qualitative trend is essentially similar to the case at 30˚ inclinations; however, the entire process occurs much faster [26]. Accordingly, the dissipation of heat from the hot molten matter to the cooler solid specimen is not catch up in a timely manner, and the overall motion of the molten matter along with a bulge shows faster. This is caused by the promoted gravity drag subjected to the deformable molten matter. Because of such a short-time feature, the downstream edge of the molten-solid interface does not progress significantly, and the incident flux is effectively absorbed to the exposed molten matter (probably near the adiabatic condition); thus, the volume expansion of the heated molten matter notably occurs. Consequently, flooding with the molten matter beyond the bulge will occur over time. Because of the viscous force subjected to the flooding molten matter, the overflown molten matter would, again, have a film-like shape and can be easily solidified once it "climbs over" the bulge to evolute the downstream bulge, as shown in the case of 75˚ inclination (see **Figure 3**). Lastly, because such a process occurs quickly, the top part of the bulge becomes a rounded shape and is unlikely to be sharp, as shown in the case of 90˚ inclination (see **Figure 4**), implying that fast and frequent overflowing occurred. Frequent flowing-off and resolidification resulted in a thinner molten layer at the irradiated zone. Accordingly, the reduction of the thermal inertia increases temperature, promoting quick gasification and resulting in a shorter ignition delay time.

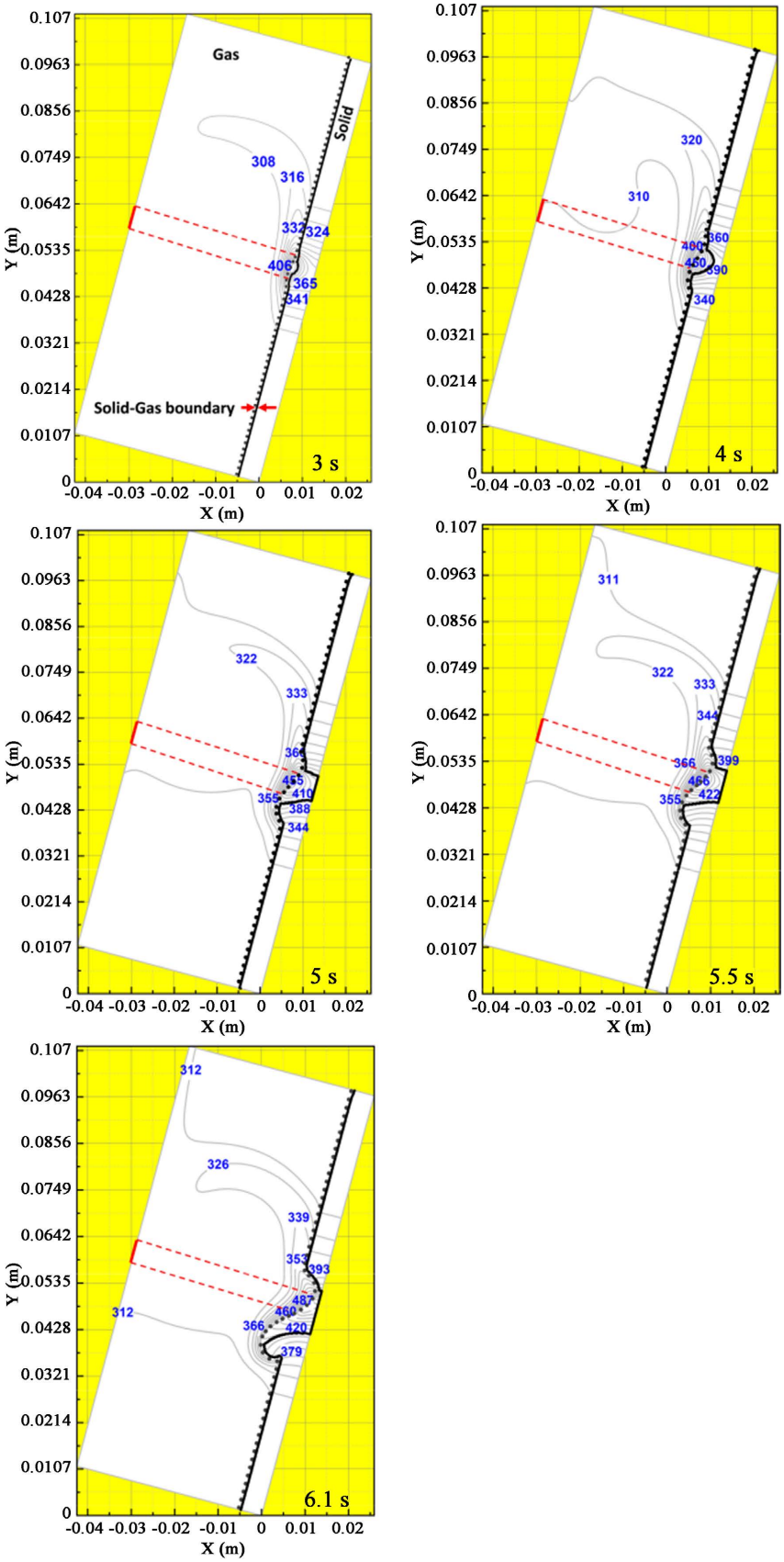

Figure 3. Temperature isotherms and melt contour for inclination of $\alpha = 75^{\circ}$.

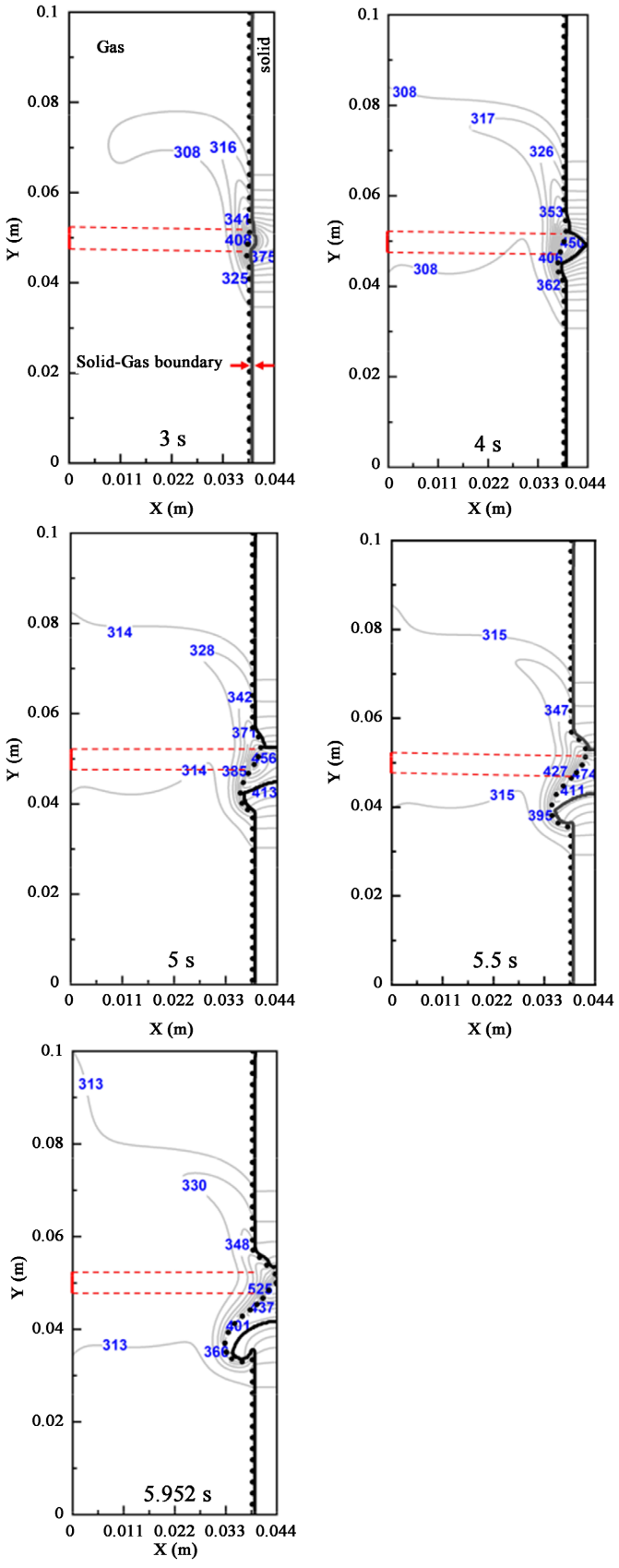

Figure 4. Temperature isotherms and melt contour for inclination of $\alpha = 90^{\circ}$.

3.3. Dripping Dynamics (Cases for Beyond 90˚)

For inclinations beyond 90˚, the overall processes seem identical with what we observed at 90˚ (see Figure 5 and Figure 6, respectively). Similarly, the formation of a bulge at the downstream edge of the heated zone occurs, preventing the downward movement of the molten matter. Nonetheless, with careful observation, notably, that several features are found only in cases, where the inclination exceeds 90˚. The growing molten matter tends to be pinched-off, likely detached (rather than sliding) over the resolidified polymer as the inclination angle increases beyond 90˚. This is obvious because gravity drag promotes such detachment motion. Accordingly, the hot molten matter does not flood over the bulge; consequently, the top of the bulge is not rounded, as found in the case at 90˚ inclination, especially at the early dripping stage (for example, 5.5 s). In the later dripping stage, when the dripping of the hot molten matter occurs, the surface tension force applied to the dripping molten matter is "pulled back" to the bulge surface, and eventually, the molten matter is "covered" over the bulge, as observed after 6 s for the case at 105˚ inclination (see Figure 5) and after 7 s for the case at 120˚ inclination (see Figure 6), respectively.

3.4. Expected Ignition Delay Time

Figure 7 plots the time history of the averaged mass fluxes issued from the heated molten matter for various inclination cases considered in this study. Here, the averaged mass flux was calculated by the total mass lost rate divided by the heated surface area. As gasification (pyrolysis) mostly occurs at the heated zone (molten matter exposed to irradiation source) in this study, the value will be treated as the representative value of mass flux in the system. To maintain the unit, for convenience, we consider the unity length in the depth direction [26]. The critical mass flux for predicting the ignitability of polymeric materials may vary, depending on the adopted inclination angles [9]; however, we will take the value of 5.0 g/m^{2}s for all angle cases for convenience. Along with this manner, the expected ignition delay time can be defined as the first moment when the local mass flux exceeds the critical value represented by black dots in the figure. As indicated, followed by the concept of the critical mass flux, an ignition event shall be identified for all inclination angle cases in this study. However, it has been already pointed out previously, under the adopted configuration used in this study, the time duration at which the mass flux exceeds the critical value is short, especially for larger angles cases (see 120˚ case). This fact implies that the ignition may not be achieved when some disturbance is added during the event in reality.

Figure 8 exhibits the predicted ignition delay time based on the definition as stated against the various angles adopted in this study. Interestingly, it is obvious that we have minimum ignition delay time at the vertical orientation case (90˚), implying that the vertical case is the most vulnerable to fire. This nonmonotonic feature on the ignition delay time versus adopted angle curve is not apparently

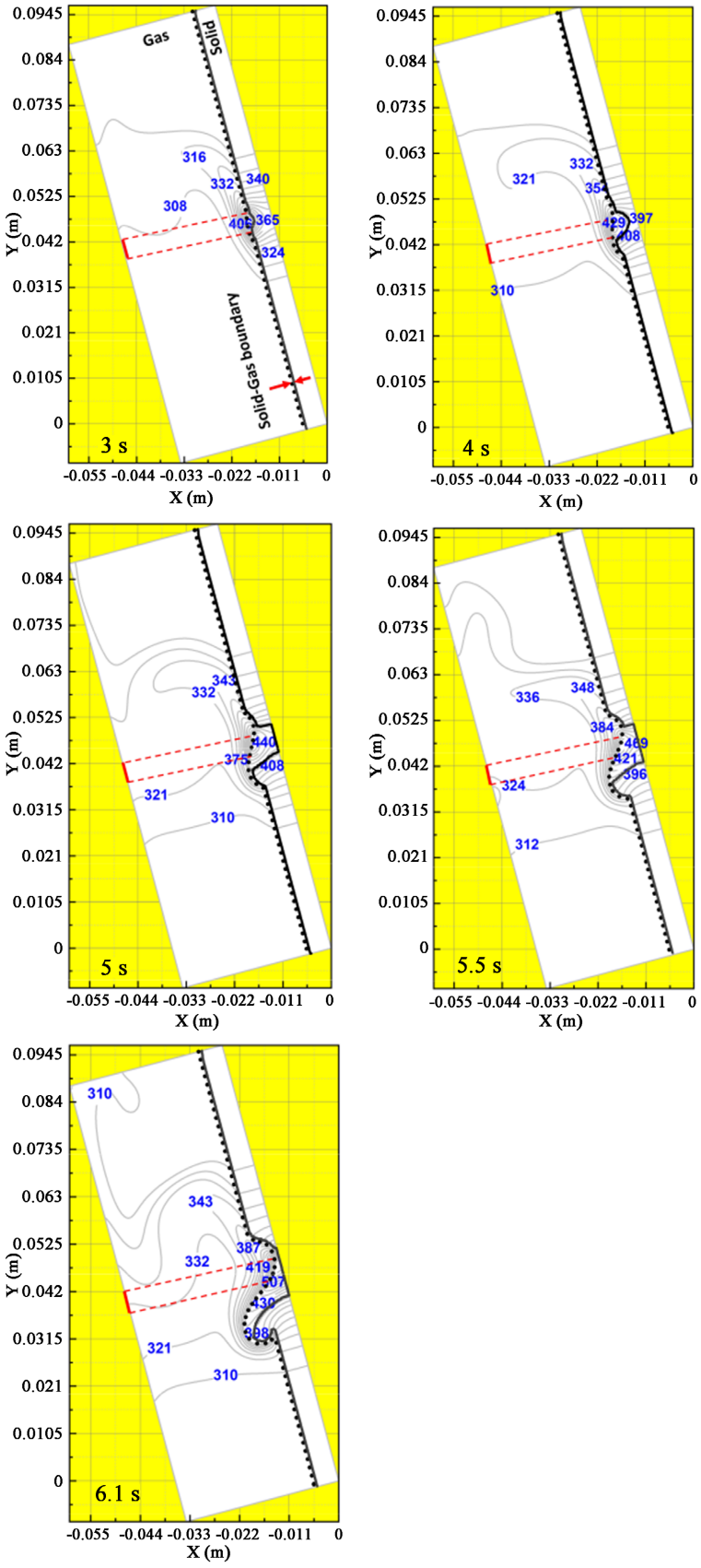

Figure 5. Temperature isotherms and melt contour for inclination of $\alpha = 105^{\circ}$.

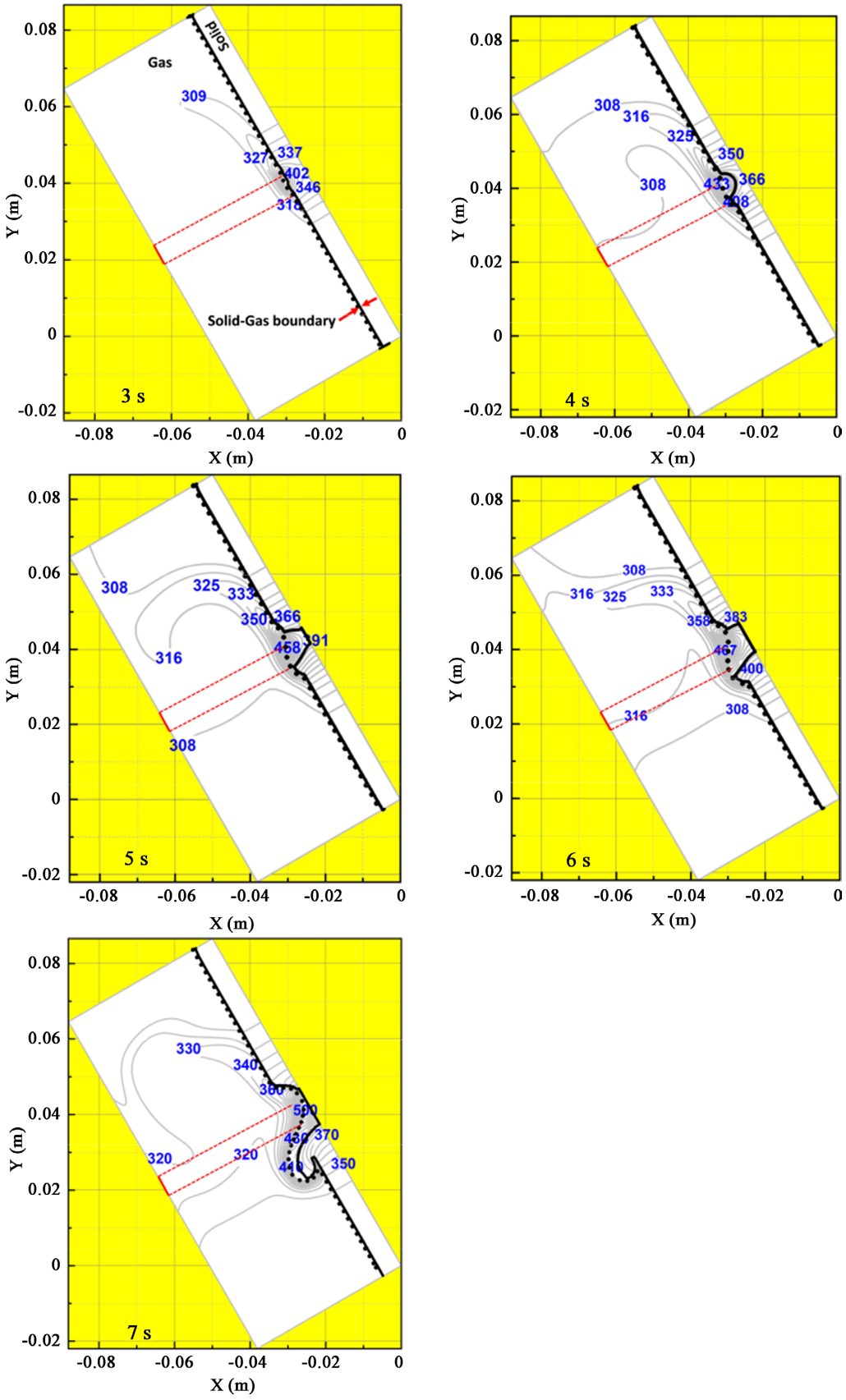

Figure 6. Temperature isotherms and melt contour for inclination of $\alpha = 120^{\circ}$.

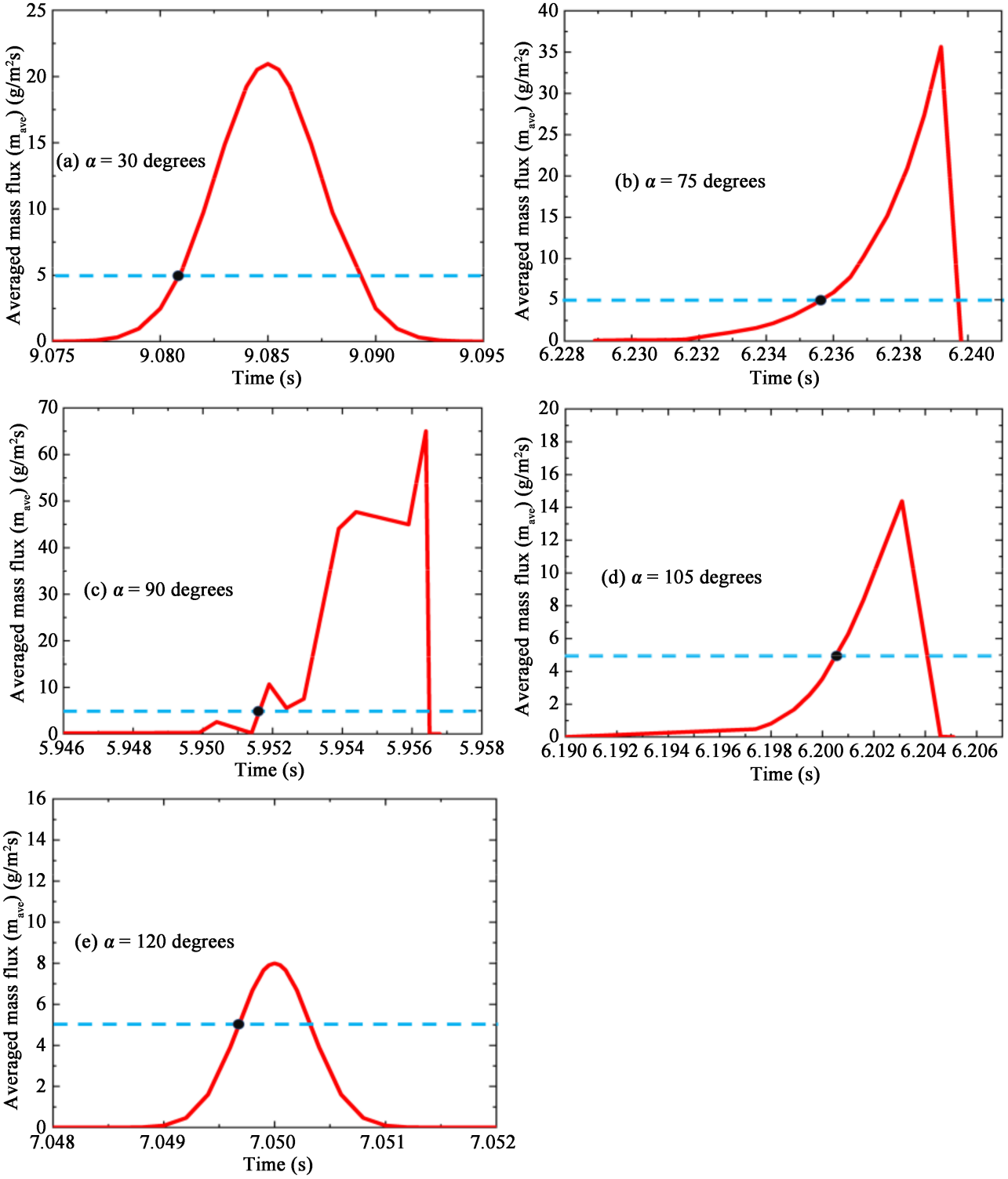

Figure 7. Time history of the averaged mass flux for various inclination cases.

observed in the experiment because of the disturbances in the system; however, such clear feature has been clarified first ever in the numerical approach which is valuable to dig into further. Let us a closer look at how this would occur in the next.

4. Discussion

As shown in Figure 8, it is quite obvious that the ignition delay time is sensitive to the adopted inclined angle. Based on our previous work [26], it is expected that the observed trend in this study may be explained by the motion of the molten matter. Accordingly, it is not difficult to imagine that the formation of the bulge at the upstream edge would play an important role in the observed trend here. Hence, in this section, we will first investigate the temporal formation of the molten matter, followed by an investigation into the formation of the bulge to provide a reasonable explanation for the observed trend shown above.

4.1. Time Variation of Volume of Dripping Matters

Figure 9 compares the growth of area (volume) of the molten matter (corresponding to the specimen whose temperature exceeds 400 K; melting temperature in this study) in time. Note that the path line is ended at the time of ignition.

As indicated in the figure, the growth of molten area (volume) increases monotonically with time, although the growth rate depends on the adopted angle. It is interesting to note that most of curves, except the cases of 30˚ and 105˚ follow a similar trend, showing that the growth increases linearly with time, so the curve follows the n^{th} power of the time ($\sim t^n$; where $1 < n < 2$). In the case of 30˚, on the contrary, the growth rate is rather weak and remains nearly constant (power n is close to unity). The most prominent feature for the case of 105˚ is that the larger molten area (volume) is maintained throughout the pre-ignition event when compared with other angle cases. This fact could be explained by two potential reasons; one is simply that the generated molten matter is pronounced under this condition, and the other is that the generated (hot) molten matter is not cooled down because of the thermal dissipation. Because the heating power is fixed throughout this study, the former reason does not appear to

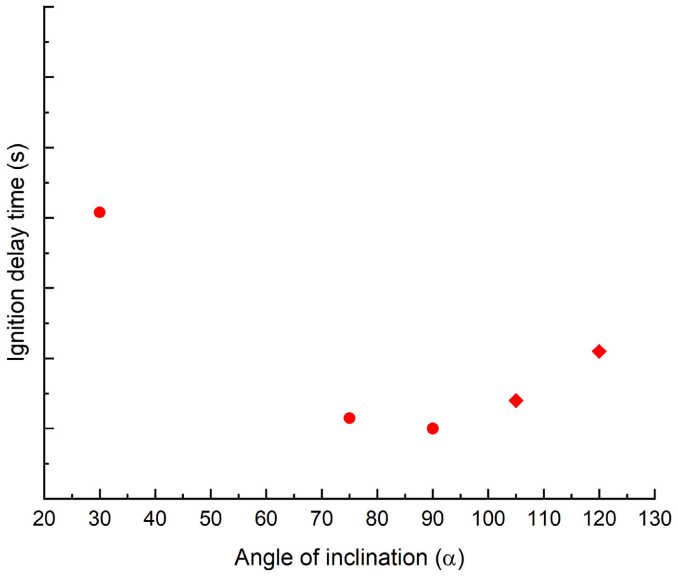

Figure 8. Ignition delay curve for various inclination cases.

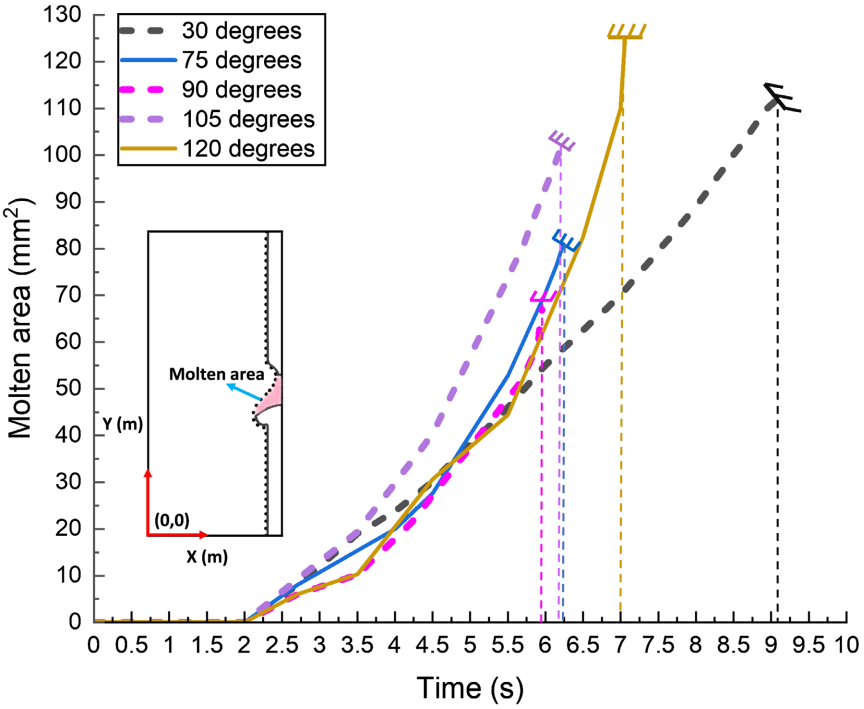

Figure 9. Pathline of Molten matter for various inclination cases.

be physical, and the latter would be a point to be addressed. Hence, thermal dissipation from hot molten matter during dripping is suggested to be an important issue causing such a trend on the ignition delay curve. Because the hot molten matter floods over the solid polymer, as shown in **Figures 2-6**, the formation of the bulge due to the resolidified process will be the first issue to be discussed in the next section.

4.2. Shape of Molten Solid Interface: Formation of "Cavity" and Growth of the "Bulge"

First, let us compare the shape of the bulge in the pre-ignition event. **Figure 10** compares the instantaneous shape of the interface of the molten and (unmelted) solid matter (whose temperature of the specimen is less than the prescribed melting temperature) at t = 5.5 s. For better comparison, all cases of the various inclination angles are overlayed into a single figure. Because the molten matter has been removed from the image, it appears that the "cavity" is formed as melting progresses because of the irradiated heating.

This figure shows several featured patterns of the melting and resolidifying processes. First, consider the downstream zone of the irradiated part. Note that, at the angle of 30˚, the specimen remains "unmelted", even at the irradiated zone, whereas the exposed area is entirely melted at the irradiated zone in other inclination cases, except for the 30˚ case. The molten matter does not significantly drip and stays there with gentle deformation in the cavity for the case of 30˚. Hence, the thermal inertia remains large to gradually increase the temperature. As the heating delay time increases and approaches the heat conduction

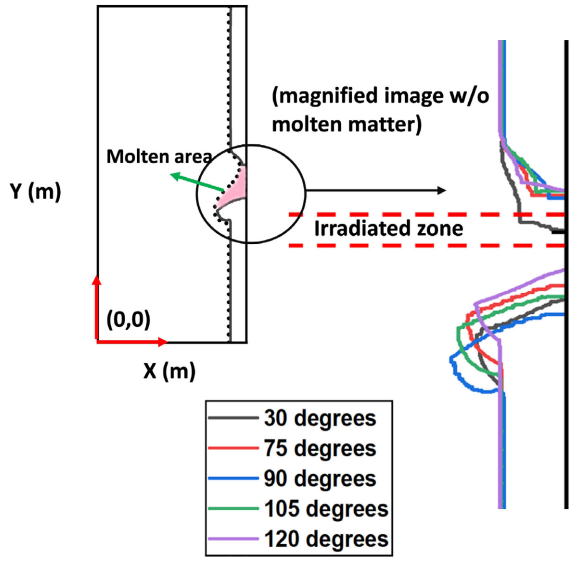

Figure 10. Instantaneous shape of the interface between molten-solid phase during the pre ignition event for various inclination cases at $t = 5.5$ s.

time, the received heat may dissipate toward the unmelted solid; thus, the molten matter tends to be cooled down. For angles above 30˚ case, by contrast, the formed molten matter begins to drip and the physical thickness of the molten matter over the irradiated zone is reduced, resulting in a rapid temperature increase. Moreover, molten matter slides over the molten-solid interface to promote heat transfer, thereby enlarging the melting zone. Similar behavior has been found in the earlier work by Kim *et al.* [20], where the heat transfer of the pinching-off molten matter would promote further melting due to enhanced convective heat transfer. Focusing on the downstream part of the irradiated zone, all cases form the bulge due to cooling of the molten matter by heat dissipation (by conduction). In other word, the bulge formation is mainly caused by the resolidified molten matter due to thermal dissipation. According to the results, it is obvious that the shape of the bulge strongly depends on the adopted inclined angles; consequently, the motion of the molten matter in the cavity will be affected because the bulge would act as a "blockage" of the dripping motion. The time variation of the characteristic quantities identifying the bulge outline should be investigated to characterize the shape of the bugle.

Figure 11 defines the two featured quantities of the bulge formed at the upstream part, such as the bulge height (h_b) and bulge angle (θ_b). These quantities are considered the potential (effective) measures for demonstrating how resolidified bulge works to prevent flooding over the molten matter in the cavity due to gravity drag. For instance, a smaller height and angle improve flooding because blocking performance against the movable molten pool in the cavity is less pronounced, whereas a larger height and angle degrade flooding vice versa. The obtained results are summarized in Figure 12.

This figure indicates that the change in the bulge angle (θ_b) is nearly identical during the melting event, except for the case of 30˚. Interestingly, θ_b eventually

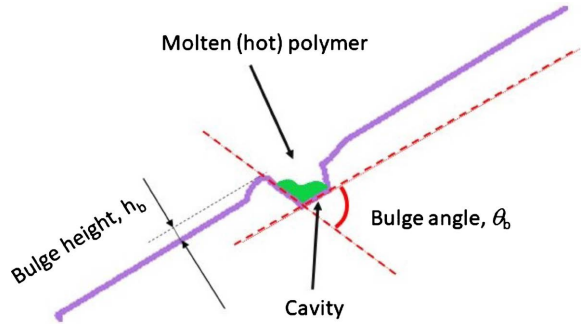

Figure 11. Physical meaning of the bulge height and angle.

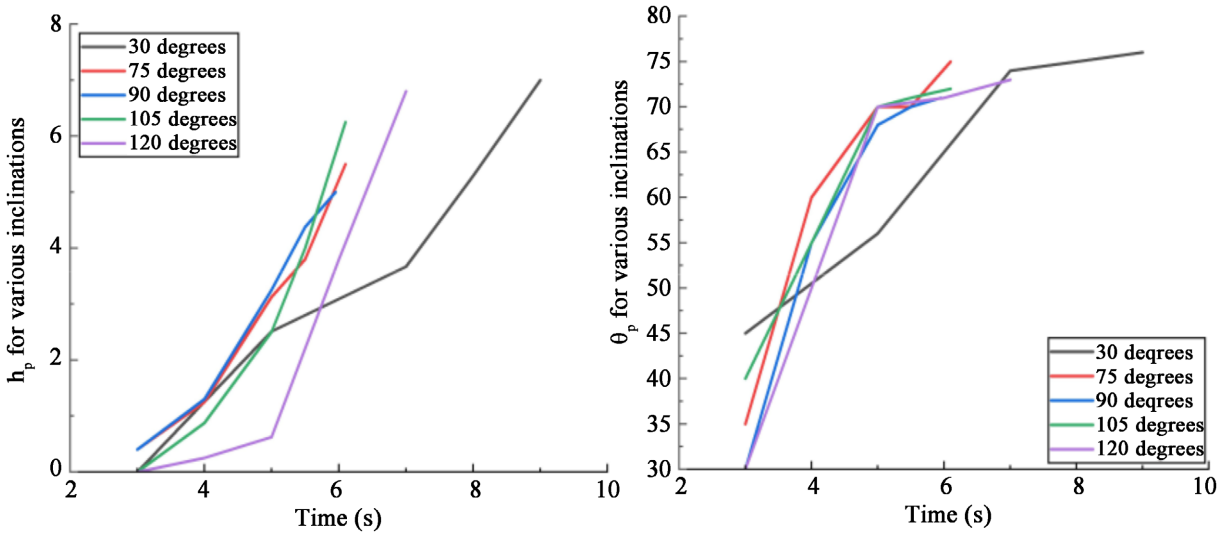

Figure 12. Calculated temporal variation of bulge height (h_b) and bulge angle (θ_b) for various inclination cases.

converges to 75˚, irrespective of the imposed inclined angles. The case of 30˚ of the inclined angle shows a gentle change of θ_b in time and slowly approaches the converged value. This is reasonable since that the relative gravity force to pull the molten matter upstream becomes less. Otherwise, θ_b rapidly evolute because of rapid melting induced by the strong irradiation exposure. Time variation of the height of the bulge (h_b), shows a monotonic change in time for all adopted inclined angle cases. This fact implies that the resolidification of the hot molten matter continuously occurs to evolute the bulge accordingly. The reason to evolute the bulge, as shown in Figures 2-6, is that the molten matter becomes a film-like shape when it overflows the bulge and is easily cooled down if the residence time of the motion is comparable with the conductive time scale (heat transfer time). Most of the inclined angle cases follow a similar trend, except for two cases, *i.e.* 30˚ and 120˚, indicating that the evolution of the bulge height slowly occurs. The gentle evolution trend for the lower inclined angle case (30˚) is expected since the external force to pull the molten matter inside the cavity over the bulge is not sufficiently high. However, the trend found in the case of 120˚ is very unfamiliar and valuable to note. As previously described, a lower bulge height means that the resolidification weakly occurs. Two potential rea-

sons would be considered for this to happen; one is that heat transfer from the hot molten matter toward the cooler solid is promoted, and the other reason is that molten matter is far from the solid interface to avoid cooling to pile up the bulge formation. Film-like molten matter over the bulge is also found, even in the case of the inclined angle at 120˚ so that the former candidate is unsuitable. Considering the gravity force direction, by contrast, some of the molten matter in the cavity will be removed (detached) from the cavity rather than sliding over the bulge. This seems more suitable to prevent the growth of the bulge height. Such detaching procedure can rapidly occur, reducing the residence time of the molten matter at the irradiation zone. It may take a (relatively) long time to be heated up to the required temperature of the irradiated molten matter.

4.3. Why Ignition Delay Increase beyond 90˚ Cases?

As previously stated, the motion of the molten matter varies in complex ways according to the adopted inclined angle. It is mainly categorized into two regimes, namely, when the inclination angle is less than 90˚ (under vertical cases: Regime I) and the other regime is when the inclination angle is greater than 90˚ (over-vertical cases; regime II). In Regime I, molten matter tends to move along/over the unmelted solid matter with the formation of the film-like layer so that significant heat exchange between the moving (hot) molten matter and the cooled unmelted solid matter is expected. Because the molten matter forms a film-like layer over the solid, the solidification process is preferred to occur, and the bulge is formed as observed. Once the bulge is formed, the motion of the molten matter is prohibited because it works as "blockage" and more time is required to overflow the bulge. Hence, a certain amount of hot molten matter remains in the cavity to increase its residence time as the irradiated zone receives energy to increase the local temperature. The thickness of the molten matter at the irradiated zone becomes thinner as the inclined angle increases, and it can easily reach the required temperature for gasification, resulting in a shorter ignition delay time. This is observed in Regime I; as the inclined angle increases, the ignition delay time decreases. In Regime II, conversely, solidification tends to be avoided since the molten matter is not always moving in tandem with the unmelted solid; rather, some of the molten matter is detached without much thermal interaction between the unmelted solid beneath it. Because of this additional degree of freedom for movement, the prohibition of the motion of the molten matter is slightly relaxed, reducing the residence time of the molten matter in the irradiated zone. This increases the time required to increase the temperature, resulting in a longer ignition delay time as the angle increases. Importantly, as shown in **Figure 7**, in the case of Regime II (cf. inclined angle is 105˚ and 120˚ in this study), besides achieving the longer ignition delay time on the basis of the critical mass flux, the peak of the achieved mass flux is lower, and the duration to show a certain mass flux is shorter. This trend is pronounced as the angle increases. This numerical fact clearly proves the impact and the effect of a shorter

residence time at the irradiated zone. Hence, we can safely confirm that the ignition is of shorter duration as the inclined angle is increased in Regime II (because of shorter residence time).

Considering the case that resolidification barely occurs (say for example, the solidification temperature is to be higher), the above-mentioned bulge formation rarely occurs, and the motion of the molten matter is not prohibited (since we do not expect to have a "blockage" effect induced by the bulge). Under such circumstances, the residence time of the molten matter cannot be increased so that the received energy from the irradiated part is easily flown off and has no chance of increasing the molten matter temperature. This will eventually decrease the chances of ignition. This fact suggests that the formation of the bulge (related to the solidification process) is effective since it could vary the motion of the molten matter from the irradiated zone. This work could demonstrate this issue using the numerical model, which could include gasification and molten dynamics simultaneously; however, it is not clearly made up so far and is difficult to verify through experiments, even when performed precisely.

5. Concluding Remarks

In this study, the potential effect of dripping and resolidification (cooling) on ignitability was numerically investigated. The numerical model comprises dripping dynamics and pyrolysis/gasification of the molten matter subjected to local heating. Dripping was promoted by adjusting the inclination of the specimen. Thus, the numerical parameter used to change the degree of dripping was the orientation of the polymeric specimen. The gas phase reaction was not considered; rather, the ignition criteria were judged by the gasification process (*i.e.*, the critical mass flux). The obtained results are summarized below. Simulation of dripping followed by gasification was successfully achieved. At lower inclinations, the slow movement of the molten matter reduces the melting rate and increases the ignition delay time. Depending on the inclination, the formed molten matter tends to drip, forming a film-like layer over the cooled (unmelted) solid. This will contribute to the "bulge" formation at the upstream edge of the molten matter, which acts as a "blockage" for the molten matter, prohibiting the overflow. This causes the residence of the molten matter at the irradiated zone to have a chance of ignition. This is the reason why the ignition delay time decreases as the inclined angle increases up to 90˚ (vertical). By contrast, for inclined angles above 90˚, the formation of a bulge is not promoted, because the molten matter tends to be detached, and does not move in tandem with the solid, and the residence time is expected to be shorter (since less blockage effect is expected). In this way, the molten matter at the irradiated zone can move quickly away from the heated zone, and the heating time increases up to the gasification temperature, resulting in a longer ignition delay time. This work successfully demonstrated the key process governing the ignition delay time, along with motion matter dynamics, using the sophisticated numerical model that can si-

mulate gasification and molten dynamics simultaneously. The systematical outcomes obtained in this work have never been achieved before and are extremely difficult to verify through experiments.

Acknowledgements

The author would like to thanks Prof. Yuji Nakamura of Toyohashi University of Technology for fruitful technical discussion.

Conflicts of Interest

The author declares no conflicts of interest regarding the publication of this paper.

References

[1] Kashiwagi, T. and Ohlemiller, T.J. (1982) A Study of Oxygen Effects on Nonflaming Transient Gasification of PMMA and PE during Thermal Irradiation. *Symposium* (*International*) *on Combustion*, **19**, 815-823. https://doi.org/10.1016/S0082-0784(82)80257-9

[2] Faraj, K., Khaled, M., Faraj, J., Hachem, F. and Castelian, C. (2021) A Review on Phase Change Materials for Thermal Energy Storage in Buildings: Heating and Hybrid Applications. *Journal of Energy Storage*, **33**, 1-33. https://doi.org/10.1016/j.est.2020.101913

[3] Kashiwagi, T. and Cleary, T.G. (1993) Effects of Sample Mounting on Flammability Properties of Intumescent Polymers. *Fire Safety Journal*, **20**, 203-225. https://doi.org/10.1016/0379-7112(93)90044-Q

[4] Kashiwagi, T. (1994) Polymer Combustion and Flammability—Role of the Condensed Phase. *Symposium (International) on Combustion*, **25**, 1423-1437. https://doi.org/10.1016/S0082-0784(06)80786-1

[5] Kashiwagi, T., Gilman, J.W., Butler, K.M., Harris, R.H., Shields, J.R. and Asano, A. (2000) Flame Retardant Mechanism of Silica Gel/Silica. *Fire and Materials*, **24**, 277-289. https://doi.org/10.1002/1099-1018(200011/12)24:6<277::AID-FAM746>3.0.CO;2-A

[6] Zhang, J., Wang, Y., Lu, X. and Yu, J. (2005) Study on Melting Behavior of Polymers during Burning. *Fire Safety Sciences*, **8**, 637-646. https://doi.org/10.3801/IAFSS.FSS.8-637

[7] Ohtani, H., Ohta, K. and Uehera, Y. (1991) Effect of Orientation on Burning Rate of Solid Combustible. *Fire and Materials*, **15**, 191-193. https://doi.org/10.1002/fam.810150406

[8] Gollner, M.J., Huang, X., Cobian, J., Rangwala, A.S. and Williams, F.A. (2013) Experimental Study of Upward Flame Spread of an Inclined Fuel Surface. *Fire Safety Sciences*, **34**, 2531-2534. https://doi.org/10.1016/j.proci.2012.06.063

[9] Peng, F., Dong, Z.X., Zhao, K., Bo, W.Z. and Zhong, Y.L. (2015) Experimental and Numerical Study on Effect of Sample Orientation on Auto-Ignition and Piloted Ignition of Poly(methyl methacrylate). *Materials*, **8**, 4004-4021. https://doi.org/10.3390/ma8074004

[10] Hu, L., Zhang, Y., Yoshioka, K., Izumo, H. and Fujita, O. (2015) Flame Spread over Electric Wire with High Thermal Conductivity Metal Core at Different Inclinations. *Proceeding of Combustion Institute*, **35**, 2607-2614.

https://doi.org/10.1016/j.proci.2014.05.059

[11] Nakamura, Y., Yoshimura, N., Matsumara, T., Ito, H., Fujita, O. and Saito, K. (2008) Flame Spread over Polymer-Insulated Wire in Reduced Pressure Environments: Similarity to Microgravity Phenomena. In: Kozo Saito, Ed., *Progress in Scale Modeling*, Springer-Verlag, Berlin, 17-27. https://doi.org/10.1007/978-1-4020-8682-3_2

[12] Nakamura, Y., Yoshimura, N., Ito, H., Azumaya, K. and Fujita, O. (2009) Flame Spread over Electric Wire in Sub-Atmospheric Pressure. *Proceeding of Combustion Institute*, **32**, 2559-2566. https://doi.org/10.1016/j.proci.2008.06.146

[13] Nakamura, Y., Yoshimura, N., Matsumara, T., Ito, H. and Fujita, O. (2009) Time-Dependent Flame Spread Behavior of Electric Wire in Sub-Atmospheric Pressure. *Proceeding of Combustion Institute*, **5**, 101.

[14] Nakamura, Y., Azumaya, K., Ito, H. and Fujita, O. (2009) Flame Spread over Electric Wire in Space Environment: Steady or Unsteady? *Proceedings of* 27*th International Symposium on Space Technology and Science*, Tsukuba, July 2009.

[15] Onate, E., Rossi, R., Idelsohn, S.R. and Butler, M.K. (2010) Melting and Spread of Polymers in Fire with the Particle Finite Element Method. *International Journal for Numerical Methods in Engineering*, **81**, 1046-1072. https://doi.org/10.1002/nme.2731

[16] Marti, J., Schartel, B. and Onate, E. (2022) Simulation of the Burning and Dripping Cables in Fire Using the Particle Finite Element Method. *Journal of Fire Sciences*, **40**, 3-25. https://doi.org/10.1177/07349041211039752

[17] Kim, Y., Hossain, A. and Nakamura, Y. (2013) Numerical Study of Effect of Thermocapillary Convection on Melting Process of Phase Change Material Subjected to Local Heating. *Journal of Thermal Science and Technology*, **8**, 136-151. https://doi.org/10.1299/jtst.8.136

[18] Kim, Y., Hossain, A. and Nakamura, Y. (2013) Chapter 23. A Numerical Study on Time-Dependent Melting and Deformation Processes of Phase Change Material (pcm) Induced by Localized Thermal Input. In: Ahsan, A., Ed., *Two Phase Flow, Phase Change and Numerical Modeling*, InTech, London, 523-540.

[19] Kim, Y., Hossain, A. and Nakamura, Y. (2013) Numerical Study of Melting of a Phase Change Material (pcm) Enhanced by Deformation of a Liquid-Gas Interface. *International Journal of Heat and Mass Transfer*, **63**, 101-112. https://doi.org/10.1016/j.ijheatmasstransfer.2013.03.052

[20] Kim, Y., Hossain, A. and Nakamura, Y. (2015) Numerical Modeling of Melting and Dripping Process of Polymeric Material Subjected to Moving Heat Flux: Prediction of Drop Time. *Proceeding of Combustion Institute*, **35**, 2555-2562. https://doi.org/10.1016/j.proci.2014.05.068

[21] Kandola, B.K., Ndiaye, M. and Price, D. (2014) Quantification of Polymer Degradation during Melt Dripping of Thermoplastic Polymers. *Polymer Degradation and Stability*, **106**, 16-25. https://doi.org/10.1016/j.polymdegradstab.2013.12.020

[22] Nakamura, Y., Kizawa, K., Mizuguchi, S., Hosogai, A. and Wakatsuki, K. (2016) Experimental Study on Near-Limiting Burning Behavior of Thermoplastic Materials with Various Thicknesses under Candle-Like Burning Configuration. *Fire Technology*, **52**, 1107-1131. https://doi.org/10.1007/s10694-016-0567-5

[23] Kobayashi, Y., Huang, X., Nakaya, S., Tsue, M. and Fernandez Pello, C. (2017) Flame Spread over Horizontal and Vertical Wires: The Role of Dripping and Core. *Fire Safety Journal*, **91**, 112-122. https://doi.org/10.1016/j.firesaf.2017.03.047

[24] Kobayashi, Y., Konno, Y., Huang, X., Nakaya, S., Tsue, M., Hashimoto, N., Fujita,

O. and Fernandez Pello, C. (2018) Effect of Insulation Melting and Dripping on Opposed Flame Spread over Laboratory Simulated Electrical Wires. *Fire Safety Journal*, **95**, 1-10. https://doi.org/10.1016/j.firesaf.2017.10.006

[25] Jiang, Y., Zhai, C. and Shi, L. (2021) Assessment of Melting and Dripping Effect on Ignition of Vertically Discrete Polypropylene and Polyethylene Slabs. *Journal of Thermal Analysis and Calorimetry*, **144**, 751-762. https://doi.org/10.1007/s10973-020-09575-1

[26] Singh, S. and Nakamura, Y. (2022) A Numerical Study of Dripping on the Ignitability of a Vertically Oriented Thermoplastic Material Locally Heated by an Irradiation Source. *Fire Technology*, **58**, 75-105. https://doi.org/10.1007/s10694-021-01137-7

[27] Nakamura, Y. and Kashiwagi, T. (2005) Effects of Sample Orientation on Nonpiloted Ignition of Thin Poly(methyl methacrylate) Sheet by a Laser 1. Theoretical Prediction. *Combustion and Flame*, **141**, 149-169. https://doi.org/10.1016/j.combustflame.2004.12.014

Nomenclature

A	Pre-exponential factor, s^{-1}
A_m	Molten area, mm^2
A_{mush}	Morphology constant, $kg/(m^3 \cdot s)$
c_p	Specific heat at constant pressure, $J/(kg \cdot K)$
E_a	Activation energy, J/mol
D	Length of irradiation wall, mm
D_{drip}	Drip diameter, mm
$\boldsymbol{F}_{ST}$	Continuum surface force per unit volume, N/m^3
g	Gravitational acceleration, m/s^2
H_g	Latent heat of vaporization, J/kg
h	Sensible enthalpy, J/kg
h_{ref}	Reference enthalpy, J/kg
I	Irradiation intensity, W/m^2
L	Latent heat of melting, J/kg
m_{ave}	Averaged mass flux, $g/(m^2 \cdot s)$
M	Total gasification rate, $kg/(m^3 \cdot s)$
M_i	Gasification in each polymeric cell, $kg/(m^3 \cdot s)$
$\boldsymbol{n}_s$	Interfacial unit normal
p	Pressure, Pa
q	Radiative heat flux, W/m^2
R	Gas constant, $J \cdot mol^{-1} \cdot K^{-1}$
T	Temperature, K
t	Time, s
Δt	Time step, s
$\boldsymbol{v}$	Bulk phase velocity, m/s
α	Angle of inclination
β	Liquid fraction
δ_s	Dirac function, 1/m
ε	Computational constant (0.001)
κ_c	Curvature of free surface, 1/m
λ	Thermal conductivity, $W/(m \cdot K)$
μ	Viscosity, Pa·s
ρ	Density, kg/m^3
σ	Surface tension coefficient, N/m
ϕ	Volume fraction

Subscripts

0	Reference
g	Gas phase
melt	Melting
m	Molten phase
mush	Mushy zone

ref	Reference
s	Solid phase
solids	Solidification
surf	Surface